Tortuosity-porosity relation in porous media flow

Maciej Matyka,[1] Arzhang Khalili,[2,3] and Zbigniew Koza[1]
[1]*Institute of Theoretical Physics, University of Wrocław, pl. M. Borna 9, 50-204 Wrocław, Poland*
[2]*Max Planck Institute for Marine Microbiology, Celsiusstrasse 1, D-28359 Bremen, Germany*
[3]*Jacobs University Bremen, Campus Ring 1, D-28759 Bremen, Germany*
(Received 28 January 2008; revised manuscript received 17 June 2008; published 25 August 2008)

We study numerically the tortuosity-porosity relation in a microscopic model of a porous medium arranged as a collection of freely overlapping squares. It is demonstrated that the finite-size, slow relaxation and discretization errors, which were ignored in previous studies, may cause significant underestimation of tortuosity. The simple tortuosity calculation method proposed here eliminates the need for using complicated, weighted averages. The numerical results presented here are in good agreement with an empirical relation between tortuosity (T) and porosity (ϕ) given by $T-1\propto\ln\phi$, that was found by others experimentally in granule packings and sediments. This relation can be also written as $T-1\propto RS/\phi$ with R and S denoting the hydraulic radius of granules and the specific surface area, respectively. Applicability of these relations appears to be restricted to porous systems of randomly distributed obstacles of equal shape and size.

DOI: 10.1103/PhysRevE.78.026306 PACS number(s): 47.56.+r, 47.15.G−, 91.60.Np

I. INTRODUCTION

In the low Reynolds number regime, flow through a porous matrix is governed by Darcy's law that links the fluid flux (discharge per unit area) $\boldsymbol{q}$ with the applied pressure gradient ∇P by the linear relation

$$\boldsymbol{q}=-\frac{k}{\mu}\nabla P, \tag{1}$$

where μ is the dynamic viscosity of the fluid and k is a proportionality constant known as permeability [1]. To a large extent, the proper description of the fluid flow through a porous medium depends on precise relations between the physical properties involved such as permeability and porosity (ϕ). In particular, much attention has been paid to deriving relations between k and ϕ [2]. In 1927 Kozeny developed a simple capillary model for a porous medium, and proposed the relation

$$k=c_0\frac{\phi^3}{S^2}, \tag{2}$$

where S is the specific surface area (the ratio of the total interstitial surface area of the voids and pores to the bulk volume) and c_0 is a dimensionless Kozeny constant that depends on the channel geometry [1]. Unfortunately, Kozeny's formula is not universal and does not hold for complicated porous geometries [1]. For example, it does not take into account pore connectivity and the fact that the specific surface area can be increased to an arbitrarily large value by removing only a fraction of the material to roughen the porous matrix surface in a fractal-like manner. On a purely physical ground, namely, one would expect that removal of the material from a porous matrix would increase its permeability, whereas Kozeny's formula predicts just the opposite [3].

One of the most widely accepted attempts to generalize relation (2) was proposed by Carman [1,4,5], who noticed that the streamlines in a porous medium are far from being completely straight and parallel to each other. This effect can be described by a dimensionless parameter T called *hydraulic tortuosity*,

$$T=\frac{\langle\lambda\rangle}{L}\geqslant 1, \tag{3}$$

where $\langle\lambda\rangle$ is the average length of the fluid paths and L is the geometrical length of the sample. Using the tortuosity, Kozeny's relation (3) can be generalized to [1]

$$k=c_0\frac{\phi^3}{T^2S^2}. \tag{4}$$

By fitting experimental data, Carman concluded that T^2 is a constant factor ($\approx 5/2$) over a wide range of porosities. Later it was found that T^2 does vary with ϕ, and can be as large as 50 for low porosity media [6,7].

Furthermore, it was realized that elongation of streamlines not only affects the hydraulic discharge, but also mediates other types of transport phenomena in the porous medium. This resulted in introducing several distinctive, experimentally measurable tortuosities obtained from a particular transport process, leading to diffusive [8,9], electrical [9–11], and acoustic [11] tortuosity definitions. There were also further theoretical attempts to define tortuosity [1,5,12]. However, all these tortuosities, in general, differ from each other and except for some very simple models [5,6,13], there is no clear consensus on the relation between them. Besides, in the literature different quantities, including T^{-1}, T^{-2}, and T^2 [1,5] have been used to denote tortuosity. Hence, to avoid confusion, here we define tortuosity through Eq. (3).

It has long since been known that flow through a porous medium depends on many factors such as porosity, tortuosity, granule shape and size distribution, saturation, Reynolds number, etc. With this many numbers of independent parameters, it is difficult to analyze the transport phenomena in a porous medium. Hence, it is essential to depart from simpler systems with a limited number of well-defined control parameters. Historically, the most successful theoretical methods of studying flows through porous media, e.g., the effec-

tive medium approximation [14,15], used a continuous approach with space-averaged variables [1,15,16]. However, more recent advances in the subject, particularly those coming from the percolation theory and computer simulations [16,17] show that the studies on a finer, microscopic level are of equally great importance. Therefore, in this paper we investigate the hydraulic tortuosity [as defined in Eq. (3)] in a creeping flow through a porous region constructed by a two-dimensional lattice system with uniformly and randomly distributed, freely overlapping solid squares. This model, first used by Koponen *et al.* [12], is simple enough to allow a numerical solution with the advantage of having porosity (ϕ) as the only control parameter.

Using the lattice gas automata (LGA) method, Koponen *et al.* [12] solved the flow equations for a porosity range of $\phi \in [0.5, 1]$, and concluded that

$$T = p(1-\phi) + 1, \tag{5}$$

where p is a fitting parameter. However, later they found this relation not being consistent with the results obtained for the porosity range $\phi \in [0.4, 0.5]$, and suggested [18] to replace it with

$$T = p\frac{(1-\phi)}{(\phi-\phi_c)^m} + 1, \tag{6}$$

in which $\phi_c \approx 0.33$ was used as the percolation threshold while p and m are some empirical parameters. Still, as an *ad hoc* formula with two fitting parameters, this relation cannot be considered a universal law. In addition, the data used to derive Eq. (6) suffer from systematic errors, as neither the impact of a finite system size nor the effect of the space discretization were taken into account.

Obviously, there is no universal relationship between tortuosity and porosity. However, for some special classes of porous media this link can exist. The aim of this paper is to carry out a detailed numerical simulation of the tortuosity-porosity relation in the model defined above, which is a relatively simple representative of the class of porous systems made of randomly distributed identical objects. We present a detailed analysis of various numerical effects influencing the accuracy of numerical computations. Because such an analysis requires large computational times and system sizes, it has often been omitted, especially in 3D simulations. However, we show that this neglect leads to serious errors. In addition, we provide a simplified algorithm for T calculation without the need for implementing complicated, weighted averages of streamline lengths.

The structure of the paper is as follows. Section II specifies the model and the numerical techniques used. Special attention is paid to the description of the nontrivial numerical technique for the tortuosity. Main results, including a detailed numerical error and finite-size analysis are provided in Sec. III. Finally, the results are discussed in Sec. IV.

II. MODEL

A. General description

The system of interest consists of a square lattice $L \times L$ lattice units (l.u.) in which a number of identical solid squares ($a \times a$ l.u.) have been placed at random locations to form a porous matrix ($1 \leqslant a \ll L$). The squares are fixed in space but free to overlap. The only restriction is that their sides must coincide with the underlying lattice. The remaining, void space is filled with a fluid. The constant, external force imposed on the porous medium is aligned with the y axis of an x-y Cartesian coordinate system to model the gravity. Following previous works [12,18], periodic boundary conditions have been imposed in both directions to minimize finite-size effects. Two examples of such porous systems are depicted in Fig. 1. The dark areas represent fixed solid obstacles, while the white part is occupied by the fluid.

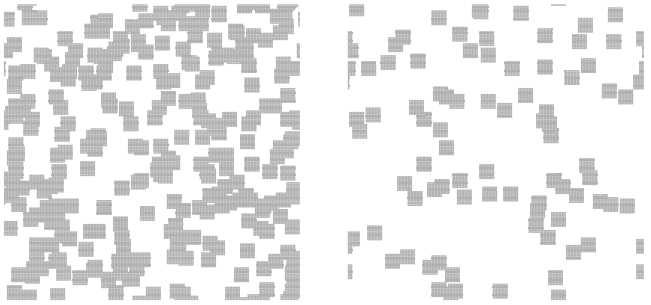

a) $\phi = 0.5$ b) $\phi = 0.8$

FIG. 1. An example of two 800×800 (l.u. $\times$ l.u.) porous matrices constructed by randomly placed and freely overlapping squares of size 10×10 (l.u. $\times$ l.u.) for two different porosities ϕ.

The value of a affects the percolation threshold ϕ_c, and hence is a relevant parameter of the model. Following [12,18], in all simulations the parameter a has been set to 10. With this choice, $\phi_c \approx 0.367$, which lies between $\phi_c \approx 0.3333$ (the continuous percolation threshold of aligned squares, $a \to \infty$) [19] and $\phi_c \approx 0.4073$ (the standard site percolation threshold, $a = 1$) [16].

B. Numerical techniques

Numerical solution of the model defined above consists of six main steps: (i) generation of a porous matrix of a known porosity; (ii) solving the flow equations in the low Reynolds number regime; (iii) finding the flow streamlines; (iv) determining the tortuosity of the flow; (v) determining the relaxation time t_{rel} and, if necessary, extrapolating the results to the stationary solution; and (vi) error analysis.

1. Construction of the porous matrix

A porous matrix of a given porosity ϕ can be generated using the method of [12,18]. Starting from an empty system, solid squares are added at random positions until the desired porosity has been reached. If the system thus generated is not permeable, it is rejected. The porosity is calculated as the fraction of unoccupied lattice nodes.

2. Lattice Boltzmann method for solving flow equations

To solve the flow equations, we applied the lattice Boltzmann model (LBM) [20] with a single relaxation time collision operator [21]. This method proved useful in microscopic

model simulations of flow through porous media for various conditions and flow regimes [2,22]. It is a numerical technique that rests on the Boltzmann transport equation discretized both in time and space, and is expressed in terms of the velocity distribution functions n_i in the form

$$n_i^{t+1}(\boldsymbol{r}+\boldsymbol{c}_i) = n_i^t(\boldsymbol{r}) + \Delta_i^t(\boldsymbol{r}) + F_i, \tag{7}$$

where $i=0,\ldots,8$ identifies lattice vectors $\boldsymbol{c}_i$, t is an integer time step, $\boldsymbol{r}$ denotes a lattice node, $\Delta_i^t(\boldsymbol{r})$ is the collision operator at $\boldsymbol{r}$, and F_i represents the ith component of the external force. We used the time unit (t.u.) equal to the LBM relaxation time which, in turn, we set equal to one LBM time step. With this choice, the kinematic viscosity $\nu = 1/6$ l.u.^{2}/t.u. [20]. This, in turn, simplifies the form of the collision operator $\Delta_i^t(\boldsymbol{r}) = n_i^{\mathrm{eq}}(\boldsymbol{r}) - n_i^t(\boldsymbol{r})$ with $n_i^{\mathrm{eq}}(\boldsymbol{r})$ being the equilibrium value of n_i at $\boldsymbol{r}$. The external force was taken into account using a method of Ref. [23]: half of the momentum was transferred directly into the equilibrium distribution function during the collision step, whereas the other half was included into the transport equation. Because we were interested in the solution of a slow, laminar flow, we utilized the equilibrium distribution function n_i^{eq} linearized in the velocity as

$$n_i^{\mathrm{eq}} = w_i\rho[1 + 3(\boldsymbol{u}\cdot\boldsymbol{c}_i)], \tag{8}$$

in which $\boldsymbol{u}$ is the macroscopic velocity vector and w_i are some weighting coefficients that depend on the lattice structure and dimension [24,25].

One problem with the LBM method is that it is incapable of resolving the macroscopic Navier-Stokes equations for channels narrower than about four lattice units [20]. This limitation becomes particularly important at low porosities, for which the number of very narrow passages increase enormously. To bypass this problem, a standard numerical mesh refinement procedure was used. Starting from the original lattice taken to generate the porous matrix, each of its L^2 elementary quads were subdivided into $k_{\mathrm{ref}}\times k_{\mathrm{ref}}$ smaller quads with $k_{\mathrm{ref}}=1,2,\ldots$ being the refinement level. The resulting $k_{\mathrm{ref}}L\times k_{\mathrm{ref}}L$ computational grid of vectors $\boldsymbol{r}$ in Eq. (7) will then be formed from the centers of the small quads. With this choice, the identification of the interface between the porous matrix and the free space is facilitated. Note that the refinement effectively increases the number of the lattice nodes between any two points by the factor k_{ref}, and that the smallest channel width is $k_{\mathrm{ref}}+1$ lattice units.

After initialization, the LBM computational loop of advection and collision continued for $t_{\max}$ time steps. The criterion for the selection of the value of $t_{\max}$ is discussed in Sec. III below. By using the midgrid bounce-back rule applied to the no-slip boundaries, second-order accurate solutions, both in space and time, could be achieved [20]. An example of the velocity field calculated with this method for a low-porosity medium is shown in Fig. 2.

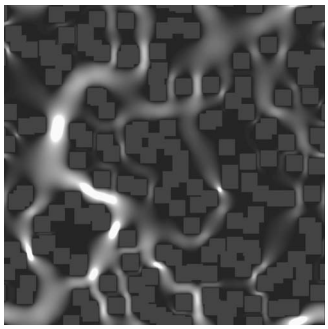

FIG. 2. Velocity magnitudes squared ($u^2=u_x^2+v_y^2$) calculated on a 600×600 numerical grid, which corresponds to a 200×200 l.u. lattice (refinement level $k_{\mathrm{ref}}=3$). The square block sizes were 10×10 l.u. (i.e., 30×30 nodes after refinement) and the porosity was $\phi=0.65$. Periodic boundary conditions were assumed in both directions. The plain gray squares represent the solid part of the medium, whereas the remaining space is open to fluid flow.

3. Flow streamlines

After obtaining the velocity field $\boldsymbol{u}$ at each grid point, the bilinear interpolation was used to define $\boldsymbol{u}(\boldsymbol{r})$ at arbitrary off-grid points $\boldsymbol{r}$. From this moment $\boldsymbol{u}$ was treated as a continuous field, and so the streamlines could be obtained by solving the equation of motion for the trajectories $\boldsymbol{r}(t)$ of massless particles [26],

$$\frac{d\boldsymbol{r}}{dt} = \boldsymbol{u}(\boldsymbol{r}). \tag{9}$$

Due to complex boundary conditions and extreme velocity variations, the fourth-order Runge-Kutta algorithm with adaptive time stepping was used [27].

4. Tortuosity

The tortuosity is defined by Eq. (3) as the ratio of the average length of all particle path lines passing through a given cross section during a unit time period to the width of the sample [1] leading to

$$T = \frac{1}{L}\frac{\int_A u_y(x)\lambda(x)dx}{\int_A u_y(x)dx}, \tag{10}$$

in which A is an arbitrary cross section of the system perpendicular to the y axis, both integrals are to be taken over all $x\in A$, $\lambda(x)$ is the length of the streamline cutting A at x, and $u_y(x)$ is the component of the velocity field at $x\in A$ normal to A. Since the stream of fluid between any pair of streamlines is constant in an incompressible flow, both integrals in Eq. (10) are independent of the cross section A. Moreover, Eq. (10) can be readily generalized to three-dimensional flows and curved surfaces A.

The integrals in Eq. (10) have been obtained in the literature either by the Monte Carlo integration [12,18,28] or by direct quadratures [6]. In the former method, the lengths of the streamlines passing through randomly chosen points within the pore volume are averaged using proper weights. In the latter method T is approximated by the relation

$$T \approx \frac{1}{L} \frac{\sum_j u_y(x_j)\lambda(x_j)\Delta x_j}{\sum_j u_y(x_j)\Delta x_j}, \tag{11}$$

where $\Delta x_j = x_{j+1} - x_j$ are discretization intervals of A. In principle, both approaches should yield the same results, but both can be easily misused. For example, some researchers used the Monte Carlo integration with streamlines passing through points chosen randomly from a uniform distribution over the whole pore space [12,28], some others calculated streamlines cutting all lattice nodes [18], whereas others recorded all streamlines crossing every lattice node along a chosen inlet plane [6,13]. However, such "uniform" approaches are not coherent with the reality of low porosity systems, in which transport is mostly carried out only through few "conducting" channels (cf. Fig. 2). Consequently, the sums in Eq. (11) contain most probably many terms of practically negligible magnitudes. To avoid this problem, we used Eq. (11) with a constant-flux constraint between two neighboring streamlines,

$$u_y(x_j)\Delta x_j = \text{const}. \tag{12}$$

The values of x_j were calculated from an implicit recursive formula

$$\int_{x_{j-1}}^{x_j} u_y(x)dx = \frac{1}{N}\int_0^L u_y(x)dx, \quad j = 1, \ldots, N, \tag{13}$$

with $x_0 = 0$. It should be noted that in case multiple solutions for Eq. (13) exist, they all correspond to the same streamline, and hence are equivalent. With this choice, Eq. (11) immediately simplifies to

$$T \approx \frac{1}{L}\frac{1}{N}\sum_{j=1}^{N} \lambda(x_j), \tag{14}$$

where N is the number of the streamlines generated. Note that all terms in this sum are of the same order of magnitude.

Thus, to calculate T, a horizontal cross section A is chosen. Next, the coordinates of the initial points x_j are determined using Eq. (13), and the corresponding streamlines are found by solving Eq. (9) in both directions until the solutions hit the system edges ($y=0$ and $y=L$). Finally, their lengths are plugged into Eq. (14).

It should be noted that not all streamlines passing through x_j cut both horizontal edges $y=0$ and $y=L$ (see Fig. 3). This may happen if the streamline generated from x_j passes through a region with extremely low fluid velocity. An example is given in Fig. 3, where arrow (a) shows an end point of an incomplete streamline. Note that this particular streamline was generated from a high-velocity region indicated by arrow (b). Arrow (c) shows a dead-end pore that coincides with the cross section A. An advantage of using a constant-flux constraint is that it minimizes the probability of choosing x_j in such stagnant regions.

To bypass the problem of incomplete streamlines, in calculation of the sum (14) only complete streamlines were taken into account. The error induced by this procedure is discussed in Sec. III.

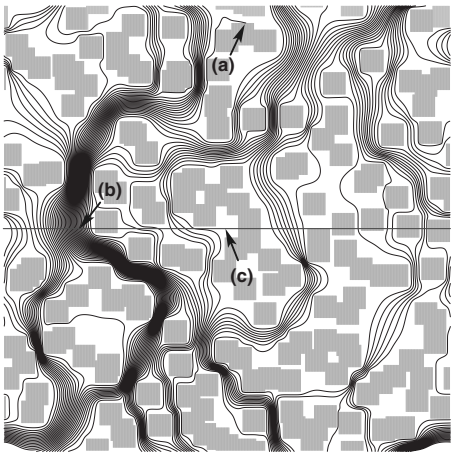

FIG. 3. Streamlines generated with the constant-flux constraint (13) for the same system as in Fig. 2 ($N=60$). The horizontal line represents the cross section $y=L/2$ on which the initial points x_j were chosen. Arrows: (a) An end point of an incomplete streamline; (b) the starting point of the incomplete streamline; and (c) a dead-end pore on the initial cross section.

5. Extrapolation to the stationary solution

Once the LBM iteration loop has been started, the solution slowly converges to the required stationary state. To determine the minimum iteration number required for obtaining the solution, we monitored the temporal evolution of the tortuosity. It turned out that after the initial stage of t_0 time steps, $T(t)$ could be approximated by

$$T(t) \approx T_s - c\exp(-t/t_{\text{rel}}), \quad t > t_0, \tag{15}$$

where $T(t)$ is defined by Eq. (14), whereas T_s, c, and t_{rel} are some ϕ-dependent parameters. We used T_s as the tortuosity at the stationary state and t_{rel} as the relaxation time to the stationary solution. The values of t_0 and t_{rel} were then used to estimate the required number of LBM iterations ($t_{\max}$).

6. Error analysis

Tortuosity values (T) calculated directly from Eq. (14) contain errors arising from different sources. While statistical errors result from randomness in the porous matrix, discretization errors appear when approximating the integrals in Eq. (10) by finite sums, and when solving flow equations by discrete lattices. Finite-size errors could emerge also as a consequence of approximating a macroscopic system with a microscopic model. Of highest importance are the errors related to the slow convergence of the numerical solution to the stationary state. Details of the error analysis are addressed in the next section.

III. RESULTS

To begin the discussion, the structure of the integrands in Eq. (10) is examined. Figure 4 shows $u_y(x)$ (relative to its maximum value $u_y^{\max} \approx 5 \times 10^{-5}$ l.u./t.u), the local tortuosity $\tau(x) = \lambda(x)/L$, their product $\tau(x)u_y(x)/u_y^{\max}$, and the ratio of the minimum to maximum trial particle speeds for the same system as in Figs. 2 and 3. All these functions depend highly

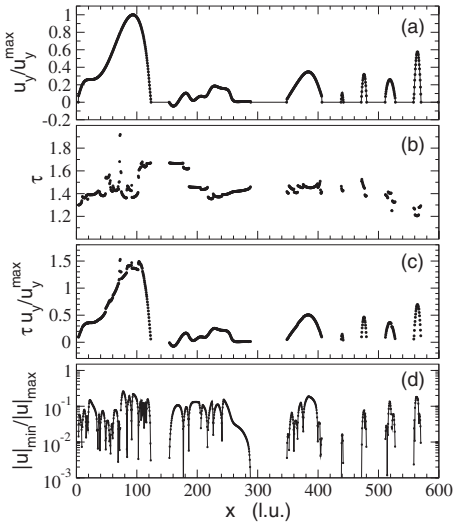

FIG. 4. The basic quantities that affect tortuosity calculation by Eq. (10): (a) Velocity component $u_y(x)$ relative to its maximum value $u_y^{\max} \approx 5 \times 10^{-5}$ l.u./t.u.; (b) local tortuosity $\tau(x) = \lambda(x)/L$; (c) the product $\tau(x)u_y(x)/u_y^{\max}$; and (d) the ratio of the minimum to maximum speeds along streamlines. All quantities were determined for the system shown in Fig. 3 with the cross section $y = L/2$ and the uniform discretization with $N = 1200$. The tortuosity for this system is $T \approx 1.45$.

on the initial cross section A, and the data for Fig. 4 were obtained from the streamlines originating at the cross section $y = L/2$. As expected, the velocity profile is continuous and piecewise differentiable, and partially resembling that of a Poiseuille (parabolic) flow. The negative value of u_y near $x = 160$ indicates that some streamlines are cutting the initial cross section many times.

In contrast to u_y, the local tortuosity τ is a discontinuous function of x [Fig. 4(b)]. Each jump in the $\tau(x)$ plot corresponds to the stream flow splitting into (or merging from) two parts upon meeting an obstacle. Thus, for a finite-size system, $\tau(x)$ is a piecewise continuous function with a certain number of discontinuities, equal to the number of "islands" existing in the porous domain. Consequently, the product $u_y(x)\tau(x)$ is also discontinuous [Fig. 4(c)]. Moreover, the problem of finding the coordinates of discontinuity points is numerically ill conditioned. These two factors greatly complicate the determination of the enumerator in Eq. (10), and introduce an additional source of errors in Eq. (14). For x_j near a discontinuity point, even small numerical errors may result in a significant jump in $\lambda(x_j)$. Two countermeasures were taken to reduce the impact of this phenomenon, which is closely related to the problem of "incomplete streamlines" discussed in Sec. II B. First, a check is made to find out how T calculated from Eq. (14) varies with N. Here, an optimal value of $N \approx L$ was found. Second, the tortuosity was calculated as an average over eight different cross sections. This approach not only reduced the error resulting from approximating Eq. (10) by Eq. (14), but also gave some estimation on its magnitude. The errors were found to be maximum for low porosities, but even for $\phi = 0.45$ the standard error of the mean was less than 0.5%.

The large number of discontinuities in $\tau(x)$ implies that the fluid velocity along a typical streamline may vary by

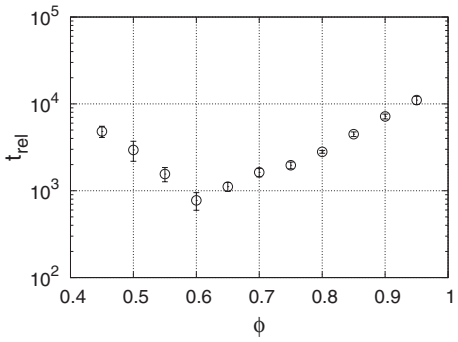

FIG. 5. Relaxation time t_{rel} as a function of porosity (ϕ) for $L = 200$ l.u., $k_{ref} = 3$, and $t_{max} = 30\,000$ t.u.

many orders of magnitude. This is shown in Fig. 4(d), in which the ratio of the minimum to maximum fluid speed (u_{min}/u_{max}) along the streamline cutting the cross section $y = L/2$ at x is plotted. In this particular case $u_{min}/u_{max} \leqslant 0.26$ and drops to 0 at all positions where $\tau(x)$ became discontinuous. A comparison of panels (a) and (d) in Fig. 4 shows that streamlines passing through a region with relatively high fluid velocity will likely hit regions where the fluid is almost stagnant. For this reason it is essential that Eq. (9) be solved with a numerical method that uses variable step lengths and local error control.

Next, we analyzed the convergence speed of the numerical results to the steady state solution. To this end, the relaxation time (t_{rel}) was calculated from Eq. (15) for all porosities investigated. As shown in Fig. 5, t_{rel} has a minimum at $\phi \approx 0.6$ and grows immediately as ϕ approaches the percolation threshold ($\phi_c \approx 0.367$) or 1. This rapid growth of the relaxation time at high porosities is a well-known property of the standard low Mach number LBM simulations [29]. On the other hand, a rapid growth of t_{rel} as ϕ approaches ϕ_c can be attributed to a growing number of larger and larger dead-end pores filled with stagnant fluid where the pressure relaxes only through diffusion, which is slow.

We found that a typical value of the initial time t_0 was between 500 and 1000 t.u. Hence, using the data from Fig. 5, we chose the number of LBM iterations as $t_{max} = 1.5 \times 10^4$ for $\phi \leqslant 0.8$ and 3×10^4 for $\phi > 0.8$. However, for the porosity $\phi = 0.45$ we observed that in several cases t_0 was significantly larger than 10^3 t.u. Closer inspection of these atypical samples revealed that their pores were arranged in a very special way: they had two conducting channels connected by another one bent in such a way that part of it was directed against the external force. Under such conditions the LBM simulations need a lot of time to distinguish such channels from nonconductive dead-end pores. Moreover, in such systems there is no reliable method to ensure that LBM simulations reach the steady state solution. Thus, even though we took all countermeasures, there is no guarantee that we actually reached the steady state in all numerical computations, and so our low-porosity results may still suffer from a small systematic error, which we estimate to be less than one percent.

Following this, finite-size effects were analyzed. Figure 6 shows the dependency of the tortuosity T on the system size L for porosities $\phi = 0.5$, 0.7, and 0.9. The lines represent fits to

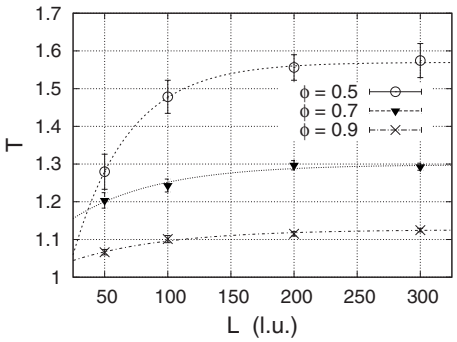

FIG. 6. Tortuosity T as a function of the system size L, for $\phi=0.5$, 0.7, 0.9, averaged over $M=25$ samples. The lines are the best fits calculated with Eq. (16). The error bars represent the standard error of the mean.

$$T(L) = T_\infty - b\exp(-cL), \tag{16}$$

where T_∞, b, and c are free parameters. These, as well as many other fits, not shown here, proved to be suitable enough to estimate the tortuosity of an infinite system T_∞. This procedure also enabled us to estimate a characteristic system length L^* above which T does not change significantly with L. It turned out that $L^* \approx 200$ for the whole porosity range. In all cases analyzed, T was found to be an increasing function of L. Thus, it becomes clear that ignoring finite-size effects and using $L < L^*$ would lead to an underestimation of T.

Following this, the sensitivity of tortuosity measurements to the numerical mesh refinement was examined. Figure 7 depicts the values of $T(L)$ for a low-porosity system ($\phi=0.5$) and four refinement levels $k_{\mathrm{ref}}=1,\ldots,4$. Apart from the case $k_{\mathrm{ref}}=1$ and $L=50$, the variation of T with k_{ref} is practically negligible, especially if compared with the variation in T related to randomness of the porous matrix (error bars in Fig. 7). Thus, as far as calculation of tortuosity is concerned, the mesh refinement did not seem to be of highest importance. The value of $k_{\mathrm{ref}}=1$ is acceptable, and $k_{\mathrm{ref}}=2$ should suffice in most practical situations. This value of k_{ref} is at odds with the criteria, mentioned above, for the LBM method to reconstruct the Navier-Stokes equations [20]. This can be explained by noticing that the main contribution to

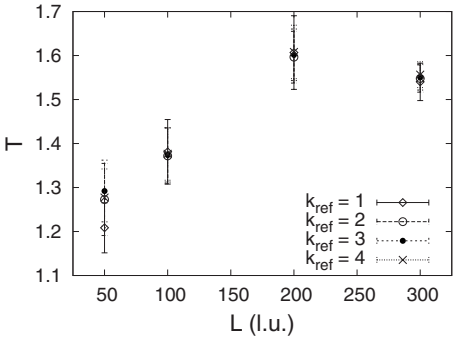

FIG. 7. The dependency of T on the system size L for $\phi=0.5$ and four refinement levels k_{ref} (symbols). Each point represents an average over nine samples.

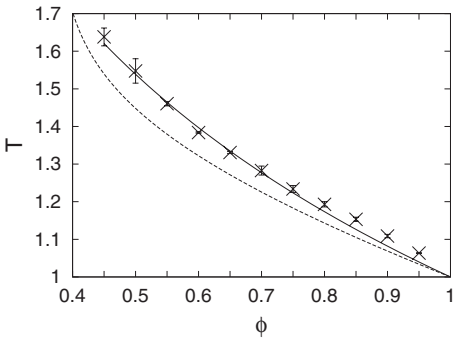

FIG. 8. The dependency of the tortuosity T on the porosity ϕ. Our data obtained with the LBM method and Eqs. (14) and (15) (cross symbols with error bars); relation (6) derived for the same system by Koponen *et al.* (dashed line); the best fit to Eq. (17b) (solid line).

tortuosity comes from broad channels, for which mesh refinement is less important. Such broad channels may not exist close to the percolation threshold, in which case $k_{\mathrm{ref}}=3$ should be used.

After finding the minimal requirements on the mesh refinement level k_{ref}, the optimal number of time steps $t_{\max}$, and the system size L^*, the tortuosity-porosity relation could be determined. For a given $\phi=0.45,0.5,\ldots,0.95$, a system size of $L=L^*$ and a refinement level of $k_{\mathrm{ref}}=3$ were chosen. At each ϕ, T was calculated for M porous matrices, with M ranging from 25 (for $\phi=0.95$) to 100 (for $\phi=0.45$), and the results are shown as cross symbols in Fig. 8. For comparison, we also plotted the best-fit curves obtained for exactly the same system by Koponen *et al.* [18] [see Eq. (6)]. Obviously, the results of Koponen *et al.* lie significantly below those obtained by us. This is due to the fact that in the work of Koponen *et al.*, a rather small system ($L<L^*$) was considered without analyzing the relaxation time. Hence, the discrepancy can be explained as a consequence of finite-size effects, large relaxation times, and discretization errors, which were not analyzed in their study.

We fitted our data to four tortuosity-porosity relations proposed by other researchers as follows:

$$T(\phi) = \phi^{-p}, \tag{17a}$$

$$T(\phi) = 1 - p\ln\phi, \tag{17b}$$

$$T(\phi) = 1 + p(1-\phi), \tag{17c}$$

$$T(\phi) = [1 + p(1-\phi)]^2, \tag{17d}$$

where p is a parameter. The first of them was proposed for the electric tortuosity by Archie [30]. The second equation was found, through variational arguments, in several theoretical studies on diffusive transport in porous systems composed of freely overlapping spheres ($p=1/2$) [31,32] or various arrangements of cylinders ($p=1$ or $p=2/3$) [33]. The same relation (with $p\approx 0.86$ and $p\approx 1.66$) was also reported in measurements of the hydraulic tortuosity for fixed beds of parallelepipedal particles with different thickness-to-side ratios [34], and in recent measurements of electrical tortuosity

in fixed beds and suspensions of glass spheres [35]. Equation (17c) is an empirical relation found for sandy ($p=2$) or clay-silt ($p=3$) sediments [36]. Finally, Eq. (17d), with $p=32/9\pi\approx 1.1$, was recently obtained in a model of the diffusive tortuosity in marine muds [37].

Although we treated p in all these formulas as an adjustable parameter, only Eq. (17b) gave a satisfactory fit for $p=0.77\pm 0.03$. This fit is plotted in Fig. 8 as a solid line. Note that for large porosities ($\phi\gtrsim 0.8$) our results are slightly larger (up to $\approx 2\%$) than the values predicted by Eq. (17b). After a closer examination, we found that this phenomenon is a consequence of applying periodic boundary conditions to domains having characteristic length scales equal to the system size. For example, if $L=100$ l.u. and $\phi=0.9$, the porous matrix is composed of only ten 10×10 squares. Under such a condition, the mean flow direction may significantly differ from the direction of the external force, violating the implicit assumption used in tortuosity equation (3) stating the parallelism of mean flow velocity and mean pressure gradient. Understanding the tortuosity as a measure of a mean elongation of the fluid particles' path as they move among solid matrices within a porous medium suggests that for systems with periodic boundary conditions Eq. (3) should be generalized to

$$T=\frac{\langle\lambda\rangle\cos\alpha}{L}, \tag{18}$$

where α is the angle between the mean fluid velocity and the external force. This equation follows from the approximation of the mean fluid displacement, as it crosses the medium, by $L/\cos\alpha$. The two definitions of tortuosity, Eqs. (3) and (18), differ by a factor $1/\cos\alpha$. We believe that this factor is responsible for the slight differences between our porosity results in Fig. 8 and those predicted by Eq. (17b). Quantitatively speaking, this would correspond to $\langle 1/\cos\alpha\rangle\lesssim 1.02$, i.e., $\langle\alpha\rangle\lesssim 11°$, which is a reasonable value for the mean deviation of a flow direction in a small system with periodic boundary conditions. The effect of $\alpha\neq 0$ appears quite small. Further detailed studies are thus necessary to understand its relevance.

The fact that our system obeys Eq. (17b) has a rather interesting and unexpected consequence. As shown previously [18], the specific surface area S [cf. Eq. (2)] in a porous system composed of freely overlapping obstacles of arbitrary shape and size in a d-dimensional space satisfies

$$S=-\frac{d}{R}\phi\ln\phi, \tag{19}$$

with R denoting hydraulic radius of obstacles ($R=a/2$ in the model studied here). With this, Eq. (17b) simplifies to

$$T-1\propto R\frac{S}{\phi}. \tag{20}$$

IV. DISCUSSION AND CONCLUSIONS

As shown by the present study, obtaining hydraulic tortuosity from numerical simulations contains many hidden problems, which may lead to incorrect conclusions. When a fluid stream hits an obstacle, it splits and then merges, causing a discontinuity in streamlines. The bounding streamline of each obstacle separates the two splitting (or merging) streams. The location of such streamlines is *a priori* not known, and the problem of finding the streamlines within those regions is numerically ill conditioned. If the system is sufficiently large, it is inevitable that majority of streamlines pass through such "ill-conditioned" regions. Moreover, the velocity magnitude along the streamlines can vary by many orders of magnitude.

At high porosities nearly each obstacle constitutes a separate "island." Although the number of discontinuities in T is very large, in general they tend to average out. At low porosities, however, severe problems may arise as discontinuities are much fewer in number (which means no "averaging out") and larger in magnitude (which results from increased island sizes).

The lattice-Boltzmann algorithm turned out adequate for studying creeping flow through porous media, especially for intermediate porosities. However, for very high or low porosities it exhibits a large relaxation time to the stationary solution, which requires special countermeasures, e.g., extrapolation. This is a known drawback of the standard LBM algorithm at high porosities, whereas for porosities close to the percolation threshold large relaxation times are inherent to the problem.

With this study we have demonstrated how sensitive tortuosity computations are to finite-size and slow relaxation effects, discretization errors, and large variation of fluid speed along streamlines. The system size must be large enough to ensure development of chaotic "splitting and merging" flows, which are characteristic for real granular systems. When periodic boundary conditions are implemented for porous domains with characteristic length scales (e.g., a typical pore size), which are of the same order as the system size itself, the mean flow direction may deviate from the direction of the external force. This is an important issue, and must be considered in the tortuosity calculations. For the porosities studied here, the mesh refinement did not turn out to be as effective in reducing discretization error as we expected. It is far more important to ensure that the numerical solution has reached the stationary solution, especially for very high or low porosities. Moreover, our results concerning large fluid velocity variations along streamlines are a clear indication for revising those tortuosity definitions which assume a constant fluid velocity along a streamline [6,13]. They also show that numerical determination of streamlines requires the use of advanced numerical integrators with adaptive step lengths and local error control.

When streamlines are generated using the constant-flux constraint, the tortuosity can be calculated simply as an average over the streamline lengths. This method reduces the computation errors and does away with the need for determining the streamlines in dead-end pores.

Obviously, there is no general relation between porosity and tortuosity. However, one may hope to establish such relations at least for some classes of porous media. The numerical data presented in this study were found to be in good agreement with Eq. (17b), obtained in previous theoretical

and experimental studies. A common denominator for all of them is a porous system made of randomly distributed obstacles of equal shape and size. It is thus possible that Eq. (17b) is valid for a whole class of such porous media. However, it is also possible that such a tortuosity-porosity dependency in these systems is a coincidence—after all, there are far more distinct porous systems than simple models to describe them. It should be also mentioned that Eq. (17b) cannot be applied close to the percolation threshold, where tortuosity diverges.

Finally, we found that in the model of freely overlapping squares, a very simple relation (20) holds between tortuosity, porosity and the specific surface area. This equation is closely related to Eq. (17b), and is expected to hold for all systems made of randomly distributed obstacles of equal shape and size.

ACKNOWLEDGMENT

We are grateful to the anonymous referee for directing our attention to the problem of a slow convergence rate of the LBM method to the stationary solution.

[1] J. Bear, *Dynamics of Fluids in Porous Media* (Elsevier, New York, 1972).
[2] A. Koponen, D. Kandhai, E. Hellén, M. Alava, A. Hoekstra, M. Kataja, K. Niskanen, P. Sloot, and J. Timonen, Phys. Rev. Lett. **80**, 716 (1998).
[3] A. W. J. Heijs and C. P. Lowe, Phys. Rev. E **51**, 4346 (1995).
[4] P. C. Carman, Trans. Inst. Chem. Eng. **15**, 150 (1937).
[5] M. B. Clennell, Geol. Soc. Spec. Publ. **122**, 299 (1997).
[6] M. A. Knackstedt and X. Zhang, Phys. Rev. E **50**, 2134 (1994).
[7] B. P. Boudreau, Geochim. Cosmochim. Acta **60**, 3139 (1996).
[8] Y. Nakashima and T. Yamaguchi, Bull. Geol. Surv. Jpn. **55**, 93 (2004).
[9] A. A. Garrouch, L. Ali, and F. Qasem, Ind. Eng. Chem. Res. **40**, 4363 (2001).
[10] P. B. Lorenz, Nature (London) **189**, 386 (1961).
[11] D. L. Johnson, T. J. Plona, C. Scala, F. Pasierb, and H. Kojima, Phys. Rev. Lett. **49**, 1840 (1982).
[12] A. Koponen, M. Kataja, and J. Timonen, Phys. Rev. E **54**, 406 (1996).
[13] X. Zhang and M. A. Knackstedt, Geophys. Res. Lett. **22**, 2333 (1995).
[14] D. Bruggeman, Ann. Phys. **24**, 636 (1935).
[15] S. Torquato, *Random Heterogeneous Materials* (Springer-Verlag, New York, 2002).
[16] M. Sahimi, Rev. Mod. Phys. **65**, 1393 (1993).
[17] A. D. Araújo, W. B. Bastos, José S. Andrade, Jr., and H. J. Herrmann, Phys. Rev. E **74**, 010401(R) (2006).
[18] A. Koponen, M. Kataja, and J. Timonen, Phys. Rev. E **56**, 3319 (1997).
[19] D. R. Baker, G. Paul, S. Sreenivasan, and H. E. Stanley, Phys. Rev. E **66**, 046136 (2002).
[20] S. Succi, *The Lattice Boltzmann Equation for Fluid Dynamics and Beyond* (Clarendon Press, New York, 2001).
[21] P. L. Bhatnagar, E. P. Gross, and M. Krook, Phys. Rev. **94**, 511 (1954).
[22] C. Pan, M. Hilpert, and C. T. Miller, Phys. Rev. E **64**, 066702 (2001).
[23] Z. Guo, C. Zheng, and B. Shi, Phys. Rev. E **65**, 046308 (2002).
[24] R. Verberg and A. J. C. Ladd, Phys. Rev. E **60**, 3366 (1999).
[25] X. He and L.-S. Luo, Phys. Rev. E **56**, 6811 (1997).
[26] F. H. Harlow and J. E. Welch, Phys. Fluids **8**, 2182 (1965).
[27] W. H. Press, B. P. Flannery, S. Teukolsky, and W. T. Vetterling, *Numerical Recipes: The Art of Scientific Computing* (Cambridge University Press, Cambridge, UK and New York, 1986).
[28] P. Alam, T. Byholm, and M. Toivakka, Nord. Pulp Pap. Res. J. **21**, 670 (2006).
[29] Z. Guo, T. S. Zhao, and Y. Shi, Phys. Rev. E **70**, 066706 (2004).
[30] G. Archie, Trans. Am. Inst. Min., Metall. Pet. Eng. **146**, 54 (1942).
[31] H. L. Weissberg, J. Appl. Phys. **34**, 2636 (1963).
[32] F.-G. Ho and W. Strieder, Chem. Eng. Sci. **36**, 253 (1981).
[33] D. S. Tsai and W. Strieder, Chem. Eng. Commun. **40**, 207 (1986).
[34] J. Comiti and M. Renaud, Chem. Eng. Sci. **44**, 1539 (1989).
[35] M. Barrande, R. Bouchet, and R. Denoyel, Anal. Chem. **79**, 9115 (2007).
[36] N. Iversen and B. B. Jørgensen, Geochim. Cosmochim. Acta **57**, 571 (1993).
[37] B. P. Boudreau and F. J. Meysman, Geology **34**, 693 (2006).